ACCOUNTS
of chemical research

Diazonium Functionalized Graphene: Microstructure, Electric, and Magnetic Properties

PING HUANG, LONG JING, HUARUI ZHU, AND XUEYUN GAO*

CAS Key Laboratory for Biomedical Effect of Nanomaterials and Nanosafety, Institute of High Energy Physics, Chinese Academy of Science, Beijing 100049, China

RECEIVED ON MARCH 6, 2012

CONSPECTUS

The unique honeycomb lattice structure of graphene gives rise to its outstanding electronic properties such as ultrahigh carrier mobility, ballistic transport, and more. However, a crucial obstacle to its use in the electronics industry is its lack of an energy bandgap. A covalent chemistry strategy could overcome this problem, and would have the benefits of being highly controllable and stable in the ambient environment. One possible approach is aryl diazonium functionalization.

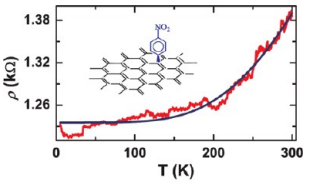

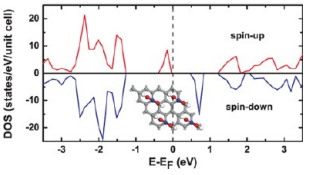

In this Account, we investigate the micromolecular/lattice structure, electronic structure, and electron-transport properties of nitrophenyl-diazonium-functionalized graphene. We find that nitrophenyl groups mainly adopt random and inhomogeneous configurations on the graphene basal plane, and that their bonding with graphene carbon atoms leads to slight elongation of the graphene lattice spacing. By contrast, hydrogenated graphene has a compressed lattice. Low levels of functionalization suppressed the electric conductivity of the resulting functionalized graphene, while highly functionalized graphene showed the opposite effect. This difference arises from the competition between the charge transfer effect and the scattering enhancement effect introduced by nitrophenyl groups bonding with graphene carbon atoms. Detailed electron transport measurements revealed that the nitrophenyl diazonium functionalization locally breaks the symmetry of graphene lattice, which leads to an increase in the density of state near the Fermi level, thus increasing the carrier density. On the other hand, the bonded nitrophenyl groups act as scattering centers, lowering the mean free path of the charge carriers and suppressing the carrier mobility.

In rare cases, we observed ordered configurations of nitrophenyl groups in local domains on graphene flakes due to fluctuations in the reaction processes. We describe one example of such a superlattice, with a lattice constant nearly twice of that of pristine graphene. We performed comprehensive theoretical calculations to investigate the lattice and the electronic structure of the superlattice structure. Our results reveal that it is a thermodynamically stable, spin-polarized semiconductor with a bandgap of ~0.5 eV.

Our results demonstrate the possibility of controlling graphene's electronic properties using aryl diazonium functionalization. Asymmetric addition of aryl groups to different sublattices of graphene is a promising approach for producing ferromagnetic, semiconductive graphene, which will have broad applications in the electronic industry.

1. Introduction

As the first purely two-dimensional material, graphene has been attracting more and more attention since its discovery in 2004.[1,2] Besides serving as a perfect two-dimensional model system for scientific interest,[3,4] it is the unique outstanding electronic properties, including ultrahigh mobility,[5] ballistic transport,[6] thinness, stability, and so forth, that inspire the graphene upsurge which aims to make it possible for the next generation nano scale electronic applications in industry.[7]

The graphene carbon atoms arrange in a honeycomb lattice in which hexagons are connected by sharing their edges so that each hexagon is surrounded by six neighboring ones. The primitive cell of the honeycomb lattice is a rhombus containing two inequivalent carbon atoms; that is, it is a compound lattice. In fact, it can be thought of as two triangular sublattices interpenetrating along one of the hexagons' edges, as shown in Figure 1a. All carbon atoms of graphene take sp^2 hybridization and covalently bond to three neighboring carbon atoms with a 120° angle between

Published on the Web 11/09/2012 www.pubs.acs.org/accounts
10.1021/ar300070a

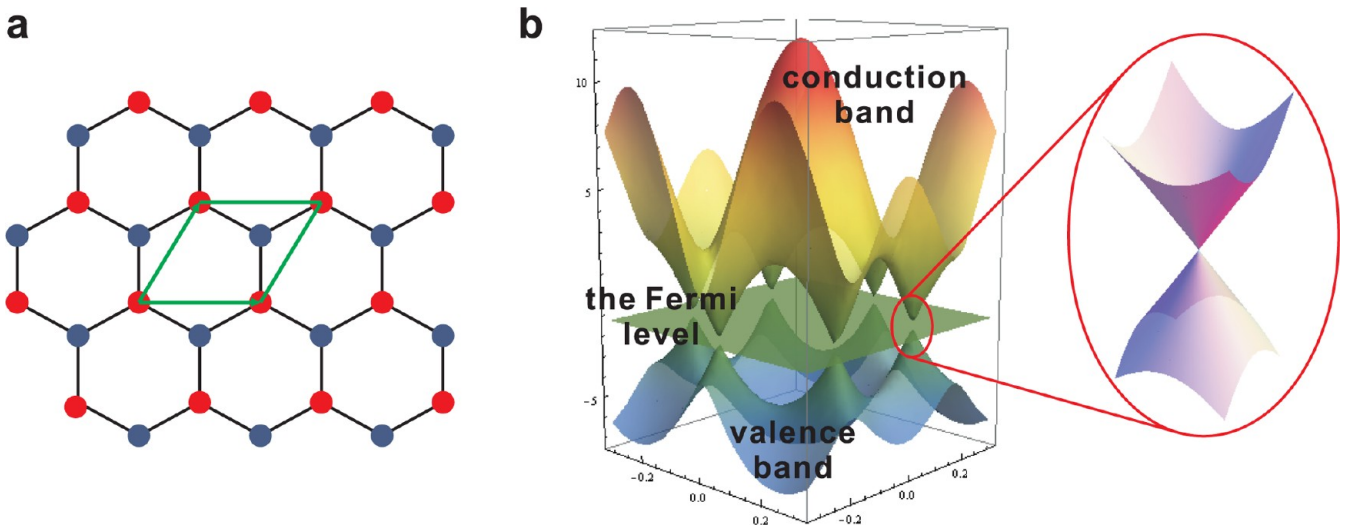

FIGURE 1. (a) Lattice structure of graphene. The rhombus indicates its primitive cell. (b) Electronic band structure of graphene. The zoom in is the linear dispersion relation near the Fermi level at the **K** point of the Brillouin zone.

SCHEME 1. Reaction Processes of Aryl Diazonium Functionalization on Graphene

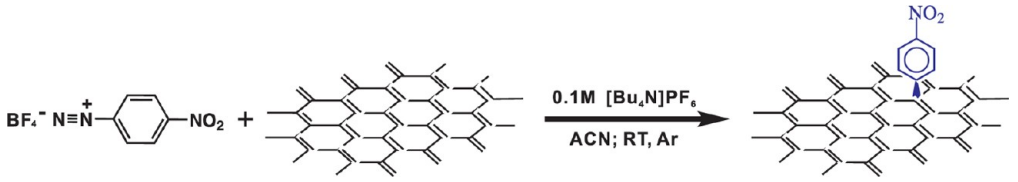

either of the two bonds. The left $2p_z$ electrons of all carbon atoms form a conjugated π-bond over the whole graphene plane.

The unique microstructure of graphene, that is, two-dimensional character and honeycomb lattice symmetry, leads to unique electronic structure and transport properties. First, the fully filled valence band and the totally empty conduction band connect with each other at the **K** and **K**′ points of the Brillouin zone as shown in Figure 1b, making graphene a gapless semiconductor.[8] Without a bandgap, graphene can be continuously tuned from p-type to n-type doping by such as an external electrostatic field, resulting in the bipolar field effect.[1] Second, the energy band is linear in the low excitation regime, leading to a zero effective mass of charge carriers.[9] This can be described by the Dirac equation in quantum electrodynamics, and thus, the charge carriers in graphene are called massless Dirac fermions.[3] Third, the sublattice symmetry introduces an extra quantum number, the pseudospin, into graphene wave functions to specify which sublattice the electron belongs to. This property is called the chirality and manifests itself in quantum transport processes such as half-integer quantum Hall effect[9,10] and unusual weak localization.[11,12]

Gapless graphene is not suitable to use in the contemporary electronic industry directly, as the on/off ratios in graphene devices are very low, leading to large static power dissipation.[7] Various approaches have been attempted to introduce a finite gap in graphene. On the physical side, applying external electric fields on bilayer graphene will open a tunable bandgap up to 250 meV,[13] and patterned absorption of atomic hydrogen onto the Moiré superlattice of epitaxial graphene results in a bandgap of 450 meV.[14] Covalent chemistry strategy is a more promising way for the stability of the functionalization toward ambient circumstance. For example, hydrogenation[15] and fluorination[16] of graphene have been realized through plasma treatment and the resulting graphene materials were insulators.

Diazonium functionalization is an alternative approach besides plasma chemistry. Aryl diazonium salts have been widely used to functionalize amorphous graphite,[17] graphite crystals,[18] carbon nanotubes,[19] and graphene.[20−27] The reduction process is illustrated in Scheme 1. Its advantages are the solution-phase reaction nature so that it is easy to realize and control, and the various choices of the grafting groups to meet different needs.[18,19] The addition of aryl groups will significantly affect the micro- and electronic

structure of graphene. First, their big sizes induce obvious steric hindrance effect, which makes their coverage on graphene much lower than that of single-atom modification. Moreover, the van der Waals interaction between those aryl groups provides a possibility to form long-range ordered superlattice structures on graphene. Then, the electronegativity of different aryl groups will lead to charge transfer either from or into the graphene basal plane, leading to p-type or n-type doping of graphene, respectively. Finally, these groups on graphene will serve as lattice defects that significantly enhance the scattering of the charge carriers, resulting in complex electric transport behaviors.

As a case study, we exhibit our systematic investigations on the nitrophenyl diazonium functionalized graphene (DFG) in this Account, including microstructures,[28] electronic structures,[29] and transport properties,[30,31] to provide a complete and clear insight into the structure–property relation of this system.

2. Microstructure of Diazonium Functionalized Graphene

The structure of the DFG from the local to global level can be characterized via atomic force microscopy (AFM), Raman spectroscopy, and transmission electronic microscopy (TEM). For the local chemical configurations, the AFM measurements revealed a height difference of 0.686 nm between pristine and functionalized graphene, which was well consistent with our density functional theory (DFT) calculations adopting the model of the nitrophenyl groups (NPs) connecting to one side of the graphene basal plane perpendicularly.[28]

The Raman spectra of the DFG, shown in Figure 2a, exhibited the D mode (at ~1350 cm^{-1}) and peaks deriving from the NPs (C–N symmetric stretching at ~1180 cm^{-1}; N–O antisymmetric stretching at ~1389, 1438, and 1515 cm^{-1}, respectively[32]) besides the G and the 2D mode of pristine graphene.[28,30] The D mode is arising from the defect-involving double resonant scattering process[33] and is the characteristics of the covalent bonds formed between graphene carbon atoms and other chemical groups.[15,34] The simultaneous appearance of the D mode and NPs' peaks directly demonstrated that the NPs connected to graphene basal plane via covalent bonds.

As a global view, two-dimensional Raman maps could provide the spacial distribution of the NPs on graphene, as shown in Figure 2b. The intensity map of the G mode indicates the distribution of the numbers of the stack layers on graphene flakes, that is, more layers exhibit stronger G

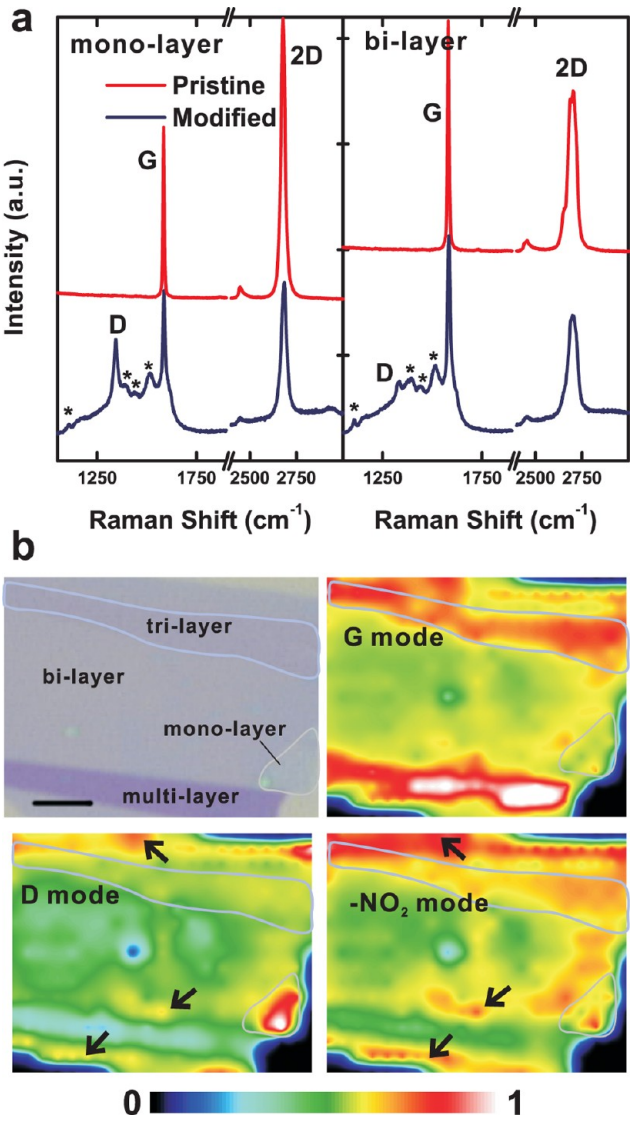

FIGURE 2. (a) Raman spectra of pristine and modified mono- and bilayer graphene. Peaks introduced by nitrophenyl groups are asterisked (*). (b) The top left panel shows the optical image of the investigated graphene sheet. The scale bar is 2.5 μm. Domains with different numbers of stack layers are outlined. In the 2D Raman maps of the G mode, D mode, and N–O vibration mode, the integrated intensity of each Raman mode is normalized. Note that the N–O vibration mode exhibits nearly the same distribution as that of the D mode, which proves that the nitrophenyl groups are bonded with graphene via σ-bonds.

mode intensity.[35] The intensity maps of the D mode and the NPs' peak, on the other hand, indicate the distribution of the covalent bonds and the NPs, respectively, which were nearly the same. Thus, the D and NPs maps both indicate the distribution of the covalently bonded NPs on graphene, which can be found quite inhomogeneous in Figure 2b. Two features can be concluded: first, the more layers stack, the fewer the NPs are; second, more NPs attach on the boundary areas, including the graphene sheet's edges as

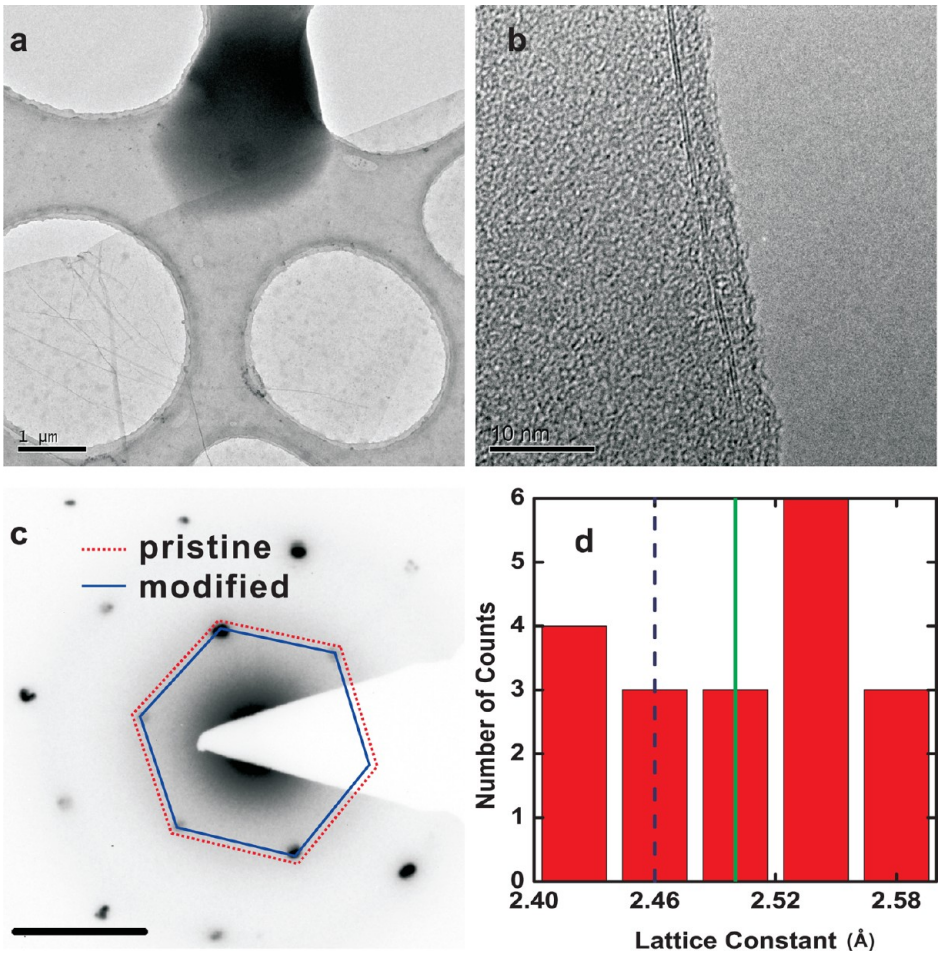

FIGURE 3. (a) Low magnification overview image of a suspended modified graphene sheet on lacey support foil. (b) High-resolution image of a modified graphene sheet near its edge. Note that the exhibition of two dark edges indicates a bilayer domain. (c) SEAD image of a modified graphene membrane. The inner and outer hexagons indicate the diffraction spots of modified and pristine graphene, respectively. Scale bar = 5 nm^{-1}. (d) Distribution of lattice constant measured in our modified graphene samples. The blue dashed and greed solid lines indicate the lattice constant of pristine and modified graphene, respectively.

well as boundaries between domains with different stack layers, than on the bulk parts. This can be attributed to the differences in the reactive ability; that is, more stack layers lead to stronger $\pi-\pi$ interaction between graphene layers which enhances the reaction barriers[23] and, on the other hand, the unsaturated dangling bonds on the boundary areas make them more reactive.[25,36]

The inhomogeneous distribution of NPs on graphene reflects the random feature of the diazonium functionalization. The combination of the random NP lattice and the graphene basal plane is expected to exhibit the global symmetry of graphene, which is demonstrated by selected area electron diffraction (SAED) investigations as shown in Figure 3c. The lattice constant can be increased up to ~5% in our measurements, and this effect was also inhomogeneous, with an average lattice constant of ~2.51 Å, while it is ~2.46 Å for pristine graphene, as shown in Figure 3d. This result is in sharp contrast with hydrogenated graphene in which the lattice compression was observed to an average of ~2.42 Å.[15] In the two effects of the covalent bonding between the NPs and the graphene basal plane, the sp^3 hybridization induced shrink of the lattice and the loosening of the conjugated π-bond induced expanding of the lattice; the latter one is dominant when the reaction extent is relatively low (compared with nearly fully hydrogenated graphene in which the former effect is dominant[15]). Note that once a carbon atom bonds with a NP, it will connect with the neighboring ones by single instead of double bonds, leading to the enlargement of the interatom spacing.[37]

3. Transport Properties of Diazonium Functionalized Graphene

The random distribution of NPs on the graphene basal plane will induce two competitive effects to its electronic

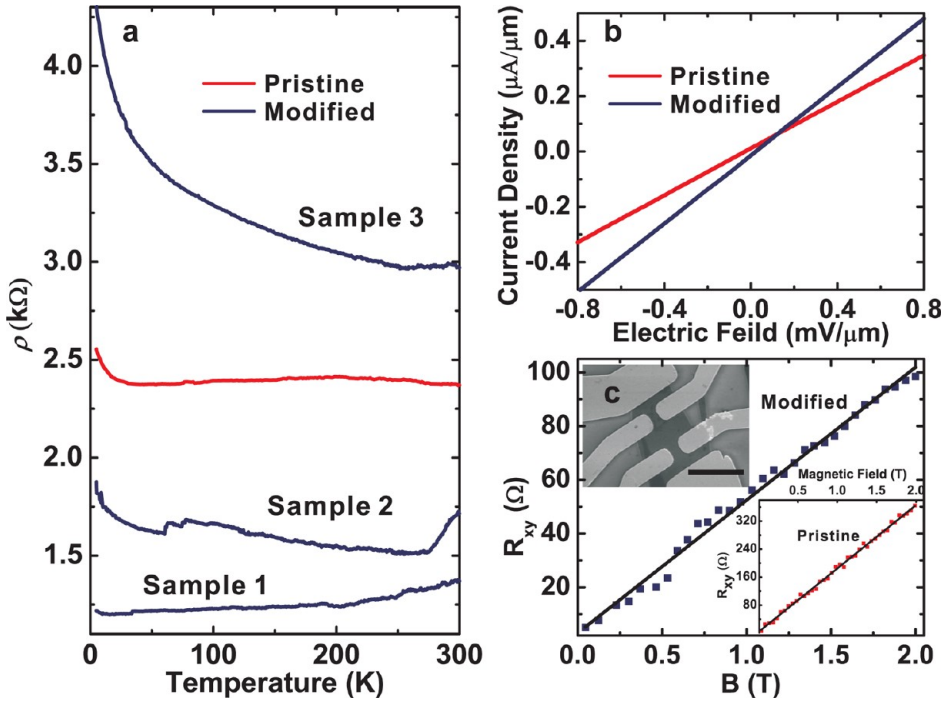

FIGURE 4. (a) $\rho-T$ character of pristine graphene and three functionalized graphene samples prepared in different reaction conditions. (b) $I-V$ character of pristine and modified graphene (sample 1). (c) Hall effect of modified graphene (sample 1). The linear fit of the data is also shown, which gives a hole density of $\sim 1.3 \times 10^{13}$ cm^{-2}. Top inset: SEM image of a Hall bar device. Scale bar = 5 μm. Bottom inset: Hall effect of pristine graphene and linear fit of the data, revealing a hole density of $\sim 3.6 \times 10^{12}$ cm^{-2}.

properties: one is the charge transfer from graphene to NPs, and the other is the decrease of the carrier mobility by enhanced scattering. With a paranitryl connecting on the benzene ring, the nitrophenyl group is a typical electron-withdrawing group, and thus, the electron cloud will be more close to the nitrophenyl groups, leading to p-type doping of the DFG. In a certain coverage range, the charge transfer induced holes density will increase with the concentrations of the NPs, and the electric conductivity of graphene will be enhanced as a result. On the other hand, however, the covalent bonding of NPs with graphene introduces defects into the system, which will increase the scattering probability of the charge carriers propagating in the DFG, and hence will suppress the electric conductivity.

Therefore, the final electronic properties of graphene are determined by the competition of the above two effects, the results of which are drastically different depending on the reaction extent. In relatively low reaction extent, the charges transferred into NPs are relatively few, so that the scattering effect is dominant, leading to suppression of the electric conductivity.[20,24,26] Once the reaction extent exceeds a certain value, the charge transfer effect will be remarkable enough to conquer the scattering effect, leading to increase of the electric conductivity. This picture has been demonstrated by our previous work,[30] as shown in Figure 4. One can find that the relatively lowly diazonium functionalized graphene (sample 3) exhibited higher resistivity than pristine graphene. Different from pristine graphene with weak temperature dependence, the resistivity of sample 3 increased monotonically on cooling below 250 K, implying a semiconductive behavior, consistent with previously reported work.[20,26] When the reaction extent was increased, as in the situation of sample 2, the resistivity was then suppressed to be smaller than that of pristine graphene. A further increase in the reaction extent led to deeper suppression of the resistivity, as in the case of sample 1. Meanwhile, the Hall effect measurement of sample 1 gave a very high hole density of $\sim 1.3 \times 10^{13}$ cm^{-2}, implying the DFG was heavily p-type doped, and the hole mobility was estimated to be $\sim$370 cm^2/(Vs), much lower than that of pristine graphene. The evaluation of the carrier density and mobility is again consistent with our picture of the effects of diazonium functionalization on graphene.

Will the enhancement of the conductivity of DFG persist with still increasing reaction extent? The answer is no. Duo to the big size of the nitrophenyl groups, however, their obvious steric hindrance effect limits their coverage on graphene; thus, let us turn to the cases of small atoms like

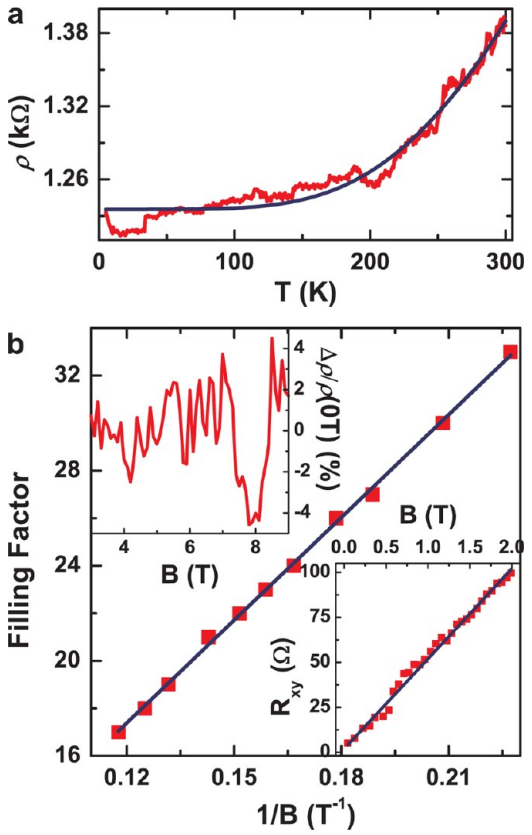

FIGURE 5. (a) $\rho-T$ characteristics of DFG, fitting curve to eq 1 is also shown. (b) Landau fan diagram of the DFG at each SdH peak and its linear fitting at 5 K, revealing an SdH oscillation frequency of $B_F \sim 146$ T, indicating a carrier density of $\sim 1.4 \times 10^{13}$ cm^{-2}. Note that the intersection is zero and means a Berry's phase of π. Top inset: SdH oscillation of the DFG at 5 K. Bottom inset: Hall effect of the DFG reveals a hole density of $\sim 1.3 \times 10^{13}$ cm^{-2}, well consistent with the SdH data.

hydrogen and fluorine. Highly hydrogenated graphene would be an insulator, and the temperature dependence of its resistivity can be described by two-dimensional variable ranges hopping, which is the transport mechanism for strongly localized systems.[15] A similar situation happens in highly fluorinated graphene.[16] In fact, as more and more graphene carbon atoms change from sp^2 to sp^3 hybridization by covalent functionalization, the electrically conductive conjugated π-bond will finally be broken down after a certain critical point at which the two-dimensional percolation phase transition occurs.[38] In this situation, free electrons that can conduct current in graphene are very low. If the H or F atoms are randomly distributed (the situations of high but not fully functionalization), the strong scattering makes the electrons localized; if the H or F atoms bond to every carbon atom, a wide gap will be opened in the energy band, as predicted by theoretical calculations.[39] Either situation will result in insulated graphene.

The transport mechanism of the DFG can be derived from further investigations,[31] as shown in Figure 5. The $\rho-T$ data can be well fitted by the Bloch–Grüneisen law which describes the temperature dependence of the resistivity of monovalent metals as well as two-dimensional electron gases:[40,41]

$$\rho(T) = \rho_0 + \alpha\left(\frac{T}{\Theta_D}\right)^5 \int_0^{\Theta_D/T} \frac{z^5}{(e^z - 1)(1 - e^{-z})}\,dz \qquad (1)$$

where ρ_0 is the residual resistivity, α is a constant and Θ_D is the Debye temperature below which only the long wave phonons are excited. The data revealed the Θ_D to be ~1840 K, slightly lower than that of pristine graphene of ~2000 K, indicating that the origin of the DFG's resistance is mainly from the phonon scattering. The resistivity of semiconductive functionalized graphene where thermal excitation is the dominant factor increases monotonically on cooling. The high intrinsic hole concentration and phonon scattering induced resistance indicate that the DFG behaved as two-dimensional hole gases (2DHGs).

The bonding of the NPs will locally break the honeycomb lattice symmetry of graphene so that the linear band structure will become nonlinear. As a result, the effective mass of the electrons in DFG will be finite rather than vanishing as in pristine graphene with linear dispersion relation. The Shubnikov–de Haas (SdH) oscillation was observed in our magnetoresistance (MR) measurements taken at 5, 10 and 50 K, as shown in Figure 5b, the temperature dependence of which can be used to estimate the electron effective mass according to the following relation:[9]

$$\frac{\Delta\rho}{\rho_0} = \frac{2\pi^2 m^* k_B T/\hbar eB}{\sinh 2\pi^2 m^* k_B T/\hbar eB} \qquad (2)$$

where $\Delta\rho$ is the amplitude of SdH oscillation, ρ_0 the resistivity without magnetic field, m^* the effective mass of electrons, k_B the Boltzmann constant, and $\hbar$ the Plank constant. The temperature evolution of the peaks at $B =$ 6.3 T and $B = 7.0$ T were fitted to eq 2, and the results revealed m^* to be $0.574m_e$ and $0.565m_e$, respectively (m_e is the mass of free electron), while experimentally derived effective mass of pristine graphene was $\sim 0.02m_e$.[9]

The effective mass determines the electrons' response to the external electric field, and virtually reflects the effect of the lattice periodic potential, which will give more detailed information about the band structure of the DFG. The density of states (DOS) can be estimated as $g(E) = g_s g_v(m^*/2\pi\hbar^2) \sim 4.8 \times 10^{11}$ cm^{-2} meV^{-1} (where g_s and g_v are the spin and

valley degeneracy, respectively), and such a giant DOS is the origin of its high intrinsic hole concentration. The Fermi velocity $v_F = \hbar k_F/m^*$ was then $\sim 1.4 \times 10^5$ m/s (where k_F is the Fermi wave vector), one magnitude lower than that of pristine graphene (which is 1×10^6 m/s),[3] indicating that the local band structure of the DFG is indeed like a two-dimensional hole gas.

On transport parameters, the mean free path $l = h/2e^2k_F\rho$ is ~10 nm. Meanwhile, the defect domain size of graphene can be empirically estimated from Raman spectrum via $L_D(\text{nm}) = 2.4 \times 10^{-10}(\text{nm}^{-3})\cdot\lambda^4(\text{nm}^4)\cdot I_G/I_D$, where λ is the excitation wavelength and I_G and I_D are the intensity of the G and the D mode, respectively.[42] The Raman spectrum of the DFG revealed a domain scale of $L \sim 8.9$ nm, well consistent with the mean free path, implying the defects induced by covalent bonding with NPs was the origin of the enhanced elastic scattering in the DFG. Since the carrier mobility is positively dependent to the mean free path, it is the significant suppression of the mean free path that leads to suppression of the carrier mobility.

Although nitrophenyl diazonium functionalization of graphene can hardly lead to thorough localization of the charge carriers due to the limitation in the coverage, clear weak localization phenomenon was still observed in the DFG.[31] Weak localization is arising from the constructive interference of electron waves propagating along two time-reversal symmetric closed paths, that is, clockwise and counterclockwise around a closed path, as illustrated in the inset of Figure 6. The constructive interference enhances the possibility of electron waves propagating to the origin, so that it adds a positive correction to the semiclassical resistivity. Weak localization will manifest itself as a peak in a MR plot around zero field, since the phase coherence of electrons can be destroyed by an external magnetic field, as shown in Figure 6. Weak localization in DFG needs more investigation because it is the middle state between ideal defect-free graphene and totally disordered functionalized graphene. The knowledge of this state will significantly benefit the understanding of how graphene transforms from semimetal to insulator, especially the breakdown process of the conjugated π-bond.[44]

4. Long Range Ordering of Nitrophenyl Groups on Functionalized Graphene

Is it possible for the NPs forming long-range ordered patterns on graphene basal plane? Due to the high-rate reaction kinetics, generally the NPs take random distribution since

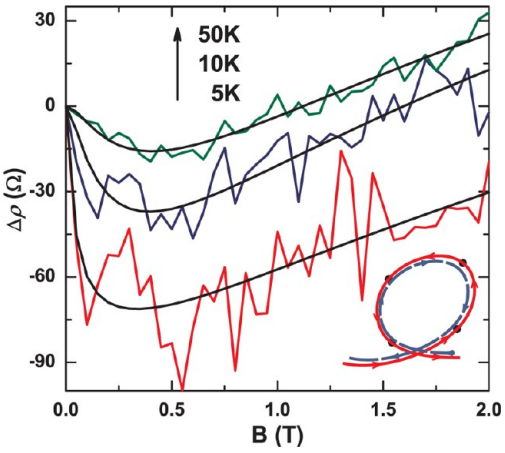

FIGURE 6. Weak localization of diazonium functionalized graphene in 5, 10 and 50 K. Smooth lines are fits according to formula given in ref 43. Inset: illustration of interference of time-reversal paths that induces weak localization.

the equilibrium state of long-range ordered arrangement could not be achieved in as-prepared DFG in a global view. Fluctuations, however, may lead to long-range ordering in *local domains*, although the possibility is ultrasmall. There are many factors that could induce fluctuations of the reaction, including local thermal excitation, inhomogeneity of the reagent solution, the corrugations of the graphene sheet, and so on. Figure 7a shows the SAED pattern of a DFG that exhibit superlattice structure with lattice constant ~5.3 Å, nearly twice of the pristine ones'. This pattern can be viewed as *AA* stacking of two lattices: one is the graphene basal plane and the other is the long-range ordered NPs that attached at only one of the graphene sublattice, as illustrated in Figure 7b.

Density functional theory (DFT) calculations were carried out based on this structure and its allotropes with the same coverage.[29] Ordinary general gradient approximation (GGA) method revealed a positive increment in the total energy after the formation of all these long-range ordered structures, implying they are thermodynamically unstable. But one should note that the $\pi-\pi$ interaction between aryl groups is not obscure when they are in such a near distance. The DFT+LAP method[45] was then adopted to take into account the van der Waals interaction between NPs, and thermodynamically favorable binding energies were obtained.

Figure 8 shows the spin-polarized DOS of the superlattice structure. A bandgap of ~0.5 eV can be found near the Fermi level. The gapless band structure of graphene originates from the sublattice symmetry of the honeycomb lattice, thus even if the DFG preserves the hexagonal symmetry, its primitive cell of the lattice is more complex and the sublattice symmetry is broken, as shown in Figure 7b. Symmetry always means

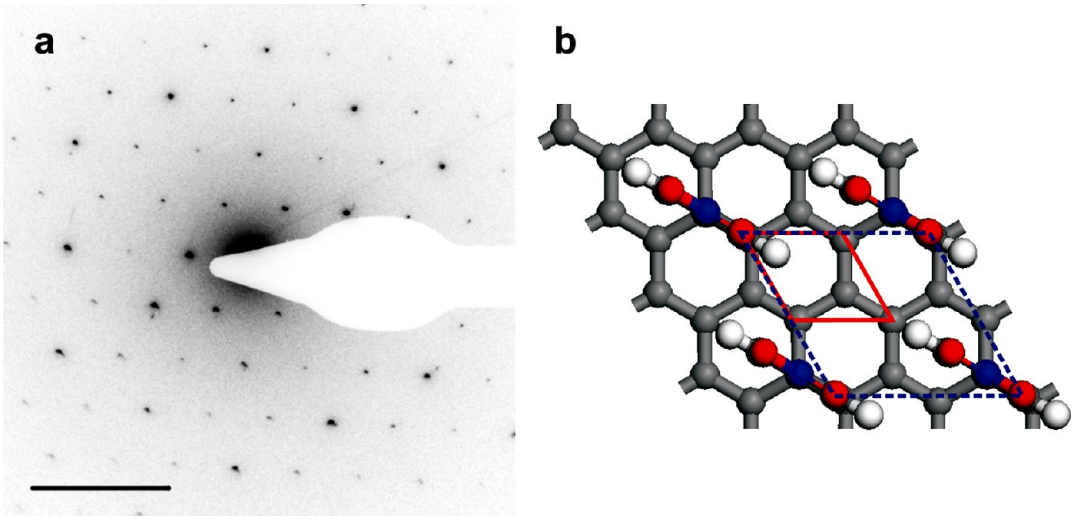

FIGURE 7. (a) SEAD pattern of diazonium functionalized graphene exhibiting superlattice structure. Scale bar = 5 nm^{-1}. (b) Illustration of the primitive cell in which the nitrophenyl groups form graphene honeycomb superlattice with twice the lattice constant of graphene. The inner and outer diamonds are guide for eyes and indicate primitive cells of pristine and modified graphene, respectively.

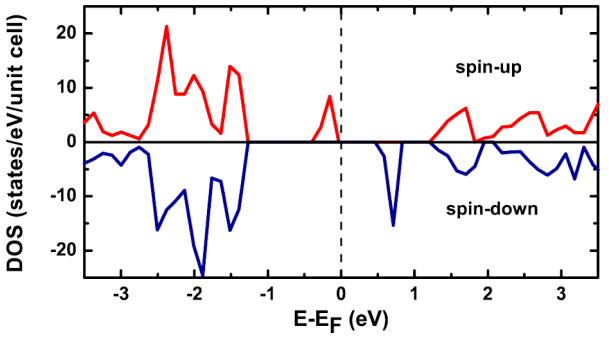

FIGURE 8. Spin-polarized DOS of diazonium functionalized graphene with NP-formed superlattice configuration. The upper panel shows the major spin (spin-up), and the lower one shows the minor spin (spin-down). An energy gap of ~0.5 eV can be found near the Fermi level due to the spin polarization.

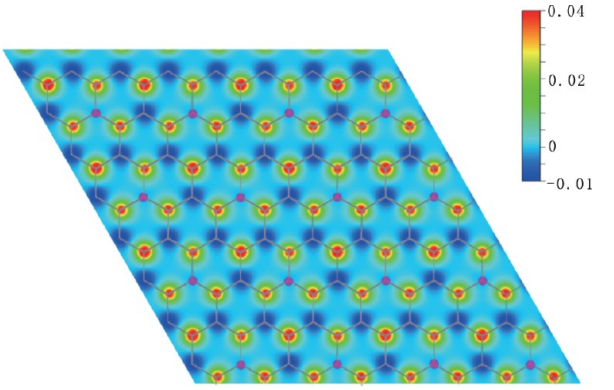

FIGURE 9. Two-dimensional distribution of spin density over the whole graphene lattice. Three periodic domains of vanishing spin, large spin-up, and small spin-down can be clearly distinguished.

degeneracy, so that the valence and conduction bands of graphene degenerate at the K point of the Brillouin zone; vice versa, symmetry breaking always means degeneracy lifting, and that is why a finite bandgap is opened in the long-range ordered DFG.

What's more amazing is that the ortho-configured NP superlattice will lead to spin polarization, which is quite promising for inducing ferromagnetism in graphene, as shown in Figure 8. One can find that the DOS of the major spin (spin-up) and that of the minor spin (spin-down) are quite different near the Fermi level. The spin-up band is fully filled while the spin-down band is totally empty, revealing a finite magnetic moment of ~1 μ_B per NP on average. The net spin density is plotted over the whole graphene lattice, as shown in Figure 9. The spin density is periodically distributed on the graphene basal plane, and three domains can be distinguished. First, vanishing spin density is the basis of distribution over the whole graphene plane, including all those carbon atoms bonding with NPs. Second, large spin-up density can be found near the carbon atoms in the complementary sublattice of the bonded one. Third, the left carbon atoms in the bonded sublattice exhibit small spin-down density, and these carbon atoms form kagome lattice. As a result, the total spin density will be in the spin-up direction to form a spin polarized configuration and hence macro-ferromagnetism may be demonstrated in this structure. In fact, evidence for ferromagnetism has been reported in diazonium functionalized epitaxial graphene.[27]

5. Conclusions and Perspectives

This Account systematically describes our research and discoveries on the microstructure, electronic, transport, and

spin properties of nitrophenyl diazonium functionalized graphene. Our main progress is on the cases of relatively high NP coverage in random distribution, which leads to loosening of the conjugated π-bond and enhancement of the electric conductivity. Detailed calculations have also been done based on a structure of NP superlattice observed on SAED with lattice constant nearly twice of that in pristine graphene, the results of which revealed an electronic structure of spin polarized semiconductor.

As mentioned above, those unique properties of graphene originate from its unique lattice structure, especially from the sublattice symmetry; yet it also leads to difficulties in using this material in the framework of the modern electronic industry. Since large scale high quality industrial synthesis of graphene can be expected in the near future, it is more and more urgent to develop reliable technique to control electronic and transport properties of graphene before its real application in electronic industry.

One of such directions is partially breaking graphene's symmetry so that the electron and spin degeneracy can be lifted, leading to energy bandgap and ferromagnetism. To this end, aryl diazonium functionalization will be promising. The competition among thermodynamic ground state, kinetic fluctuation, and steric hindrance effect provides abundant means to design and control the lattice and electronic structures, and the observed superlattice by SEAD is such an example. Generally, asymmetric aryl groups to the graphene basal plane, that is, the aryl groups unequally bond with carbon atoms in different sublattices, will lead to breaking of the sublattice symmetry. As a result, an energy gap will open and spin configuration will be polarized. Ferromagnetic semiconductive graphene will have broad applications in spintronics.

Although various structures of aryl diazonium functionalized graphene can be designed to achieve various properties by theoretical calculations, it is still very difficult to control its real structures in experiments so far. More and deeper investigations are needed on how to synthesize asymmetric and/or long-range ordered aryl diazonium functionalized graphene over crystal scale.

We are deeply grateful to our experimental and theoretical collaborators for their technical support and/or valuable discussions. The work described in this Account was supported financially by the National Key Basic Research Program of China (Grant Nos. 2013CB932703, 2013CB933704, 2011CB933400, 2010CB934004, 2009CB930204) and the Natural Science Foundation of China (Grant Nos. 31271072, 31070891, 30900302, 30870677).

BIOGRAPHICAL INFORMATION

Ping Huang received his master's degree in condensed matter physics at Wuhan University in 2008. He is now an assistant research fellow at the Institute of High Energy Physics (IHEP), Chinese Academy of Science (CAS). His current research interests are electronic and transport properties of low dimensional systems.

Long Jing graduated from the University of Science and Technology of China. He is now an assistant research fellow at IHEP. His current research interests are electronic structures of nanomaterials by the first principle calculations and assembly processes of them by molecular dynamics simulation.

Huarui Zhu received her master's degree in 2008 at Beijing Normal University. She is now an assistant research fellow at IHEP. Her current research interests are in the area of synthesis, functionalization, and characterization of nanomaterials, especially carbon nanotubes and graphene.

Xueyun Gao received his Ph.D. degree in 2003 from Institute of Solid State Physics, CAS. From 2004 to 2007, he was a visiting scholar in City University of New York City and University of Illinois at Urbana and Champaign. After 2007, he was a group leader in the CAS key lab in the Institute of High Energy Physics. His first interest is chemical approaching and physical understanding of graphene, and clusters in bioimaging is his second interest. He has a copatented industry product and has published 30 more research papers.

FOOTNOTES

*To whom correspondence should be addressed. E-mail: gaoxy@ihep.ac.cn.
The authors declare no competing financial interest.

REFERENCES

1 Novoselov, K. S.; Geim, A. K.; Morozov, S. V.; Jiang, D.; Zhang, Y.; Dubonos, S. V.; Grigorieva, I. V.; Firsov, A. A. Electric Field Effect in Atomically Thin Carbon Films. *Science* **2004**, *306*, 666–669.

2 Geim, A. K.; Novoselov, K. S. The rise of graphene. *Nat. Mater.* **2007**, *6*, 183–191.

3 Neto, A. H.; Guinea, F.; Peres, N. M.; Novoselov, K. S.; Geim, A. K. The electronic properties of graphene. *Rev. Mod. Phys.* **2009**, *81*, 109–54.

4 Das Sarma, S.; Adam, S.; Hwang, E. H.; Rossi, E. Electronic transport in two-dimensional graphene. *Rev. Mod. Phys.* **2011**, *83*, 407.

5 Morozov, S. V.; Novoselov, K. S.; Katsnelson, M. I.; Schedin, F.; Elias, D. C.; Jaszczak, J. A.; Geim, A. K. Giant Intrinsic Carrier Mobilities in Graphene and Its Bilayer. *Phys. Rev. Lett.* **2008**, *100*, 016602.

6 Miao, F.; Wijeratne, S.; Zhang, Y.; Coskun, U. C.; Bao, W.; Lau, C. N. Phase-Coherent Transport in Graphene Quantum Billiards. *Science* **2007**, *317*, 1530–1533.

7 Avouris, P. Graphene: Electronic and Photonic Properties and Devices. *Nano Lett.* **2010**, *10*, 4285–4294.

8 Wallace, P. R. The Band Theory of Graphite. *Phys. Rev.* **1947**, *71*, 622.

9 Novoselov, K. S.; Geim, A. K.; Morozov, S. V.; Jiang, D.; Katsnelson, M. I.; Grigorieva, I. V.; Dubonos, S. V.; Firsov, A. A. Two-dimensional gas of massless Dirac fermions in graphene. *Nature* **2005**, *438*, 197–200.

10 Zhang, Y.; Tan, Y.-W.; Stormer, H. L.; Kim, P. Experimental observation of the quantum Hall effect and Berry's phase in graphene. *Nature* **2005**, *438*, 201–204.

11 Wu, X.; Li, X.; Song, Z.; Berger, C.; de Heer, W. A. Weak Antilocalization in Epitaxial Graphene: Evidence for Chiral Electrons. *Phys. Rev. Lett.* **2007**, *98*, 136801.

12 Tikhonenko, F. V.; Kozikov, A. A.; Savchenko, A. K.; Gorbachev, R. V. Transition between Electron Localization and Antilocalization in Graphene. *Phys. Rev. Lett.* **2009**, *103*, 226801.

13 Zhang, Y.; Tang, T.-T.; Girit, C.; Hao, Z.; Martin, M. C.; Zettl, A.; Crommie, M. F.; Shen, Y. R.; Wang, F. Direct observation of a widely tunable bandgap in bilayer graphene. *Nature* **2009**, *459*, 820–823.

14 Balog, R.; et al. Bandgap opening in graphene induced by patterned hydrogen adsorption. *Nat. Mater.* **2010**, *9*, 315–319.

15 Elias, D. C.; Nair, R. R.; Mohiuddin, T. M.; Morozov, S. V.; Blake, P.; Halsall, M. P.; Ferrari, A. C.; Boukhvalov, D. W.; Katsnelson, M. I.; Geim, A. K.; Novoselov, K. S. Control of Graphene's Properties by Reversible Hydrogenation: Evidence for Graphane. *Science* **2009**, *323*, 610–613.

16 Robinson, J. T.; Burgess, J. S.; Junkermeier, C. E.; Badescu, S. C.; Reinecke, T. L.; Perkins, F. K.; Zalalutdniov, M. K.; Baldwin, J. W.; Culbertson, J. C.; Sheehan, P. E.; Snow, E. S. Properties of Fluorinated Graphene Films. *Nano Lett.* **2010**, *10*, 3001–3005.

17 Liu, Y.-C.; McCreery, R. L. Reactions of Organic Monolayers on Carbon Surfaces Observed with Unenhanced Raman Spectroscopy. *J. Am. Chem. Soc.* **1995**, *117*, 11254–11259.

18 Allongue, P.; Delamar, M.; Desbat, B.; Fagebaume, O.; Hitmi, R.; Pinson, J.; Savéant, J.-M. Covalent Modification of Carbon Surfaces by Aryl Radicals Generated from the Electrochemical Reduction of Diazonium Salts. *J. Am. Chem. Soc.* **1997**, *119*, 201–207.

19 Bahr, J. L.; Yang, J.; Kosynkin, D. V.; Bronikowski, M. J.; Smalley, R. E.; Tour, J. M. Functionalization of Carbon Nanotubes by Electrochemical Reduction of Aryl Diazonium Salts: A Bucky Paper Electrode. *J. Am. Chem. Soc.* **2001**, *123*, 6536–6542.

20 Bekyarova, E.; Itkis, M. E.; Ramesh, P.; Berger, C.; Sprinkle, M.; de Heer, W. A.; Haddon, R. C. Chemical Modification of Epitaxial Graphene: Spontaneous Grafting of Aryl Groups. *J. Am. Chem. Soc.* **2009**, *131*, 1336–1337.

21 Lomeda, J. R.; Doyle, C. D.; Kosynkin, D. V.; Hwang, W.-F.; Tour, J. M. Diazonium Functionalization of Surfactant-Wrapped Chemically Converted Graphene Sheets. *J. Am. Chem. Soc.* **2008**, *130*, 16201–16206.

22 Hossain, M. Z.; Walsh, M. A.; Hersam, M. C. Scanning Tunneling Microscopy, Spectroscopy, and Nanolithography of Epitaxial Graphene Chemically Modified with Aryl Moieties. *J. Am. Chem. Soc.* **2010**, *132*, 15399–15403.

23 Koehler, F. M.; Jacobsen, A.; Ensslin, K.; Stampfer, C.; Stark, W. J. Selective Chemical Modification of Graphene Surfaces: Distinction Between Single- and Bilayer Graphene. *Small* **2010**, *6*, 1125–1130.

24 Sinitskii, A.; Dimiev, A.; Corley, D. A.; Fursina, A. A.; Kosynkin, D. V.; Tour, J. M. Kinetics of Diazonium Functionalization of Chemically Converted Graphene Nanoribbons. *ACS Nano* **2010**, *4*, 1949–1954.

25 Sharma, R.; Baik, J. H.; Perera, C. J.; Strano, M. S. Anomalously Large Reactivity of Single Graphene Layers and Edges toward Electron Transfer Chemistries. *Nano Lett.* **2010**, *10*, 398–405.

26 Zhang, H.; Bekyarova, E.; Huang, J.-W.; Zhao, Z.; Bao, W.; Wang, F.; Haddon, R. C.; Lau, C. N. Aryl Functionalization as a Route to Band Gap Engineering in Single Layer Graphene Devices. *Nano Lett.* **2011**, *11*, 4047–4051.

27 Hong, J.; Niyogi, S.; Bekyarova, E.; Itkis, M. E.; Ramesh, P.; Amos, N.; Litvinov, D.; Berger, C.; de Heer, W. A.; Khizroev, S.; Haddon, R. C. Effect of Nitrophenyl Functionalization on the Magnetic Properties of Epitaxial Graphene. *Small* **2011**, *7*, 1175–1180.

28 Zhu, H.; Huang, P.; Jing, L.; Zuo, T.; Zhao, Y.; Gao, X. Microstructure evolution of diazonium functionalized graphene: A potential approach to change graphene electronic structure. *J. Mater. Chem.* **2012**, *22*, 2063–2068.

29 Jing, L.; Huang, P.; Zhu, H.; Gao, X. Spin-Polarized Semiconductors: Tuning the Electronic Structure of Graphene by Introducing a Regular Pattern of sp^3 Carbons on the Graphene Plane. *Small* DOI:10.1002/smll.201201100.

30 Huang, P.; Zhu, H.; Jing, L.; Zhao, Y.; Gao, X. Graphene Covalently Binding Aryl Groups: Conductivity Increases Rather than Decreases. *ACS Nano* **2011**, *5*, 7945–7949.

31 Ping, H.; Jing, L.; Zhu, H.; Gao, X. Transport properties of diazonium functionalized graphene: chiral two-dimensional hole gases. *J. Phys.: Condens. Matter* **2012**, *24*, 235305.

32 El'Kin, P.; Pulin, V.; Kosterina, E. Structural Dynamic Models and Vibrational Spectra of Nitrobenzene and Nitropyridines. *J. Appl. Spectrosc.* **2005**, *72*, 483–487.

33 Reich, S.; Thomsen, C. Raman spectroscopy of graphite. *Philos. Trans. R. Soc.* **2004**, *362*, 2271–2288.

34 Niyogi, S.; Bekyarova, E.; Itkis, M. E.; Zhang, H.; Shepperd, K.; Hicks, J.; Sprinkle, M.; Berger, C.; Lau, C. N.; DeHeer, W. A.; Conrad, E. H.; Haddon, R. C. Spectroscopy of Covalently Functionalized Graphene. *Nano Lett.* **2010**, *10*, 4061–4066.

35 Graf, D.; Molitor, F.; Ensslin, K.; Stampfer, C.; Jungen, A.; Hierold, C.; Wirtz, L. Spatially Resolved Raman Spectroscopy of Single- and Few-Layer Graphene. *Nano Lett.* **2007**, *7*, 238–242.

36 Sun, Z.; Kohama, S.; Zhang, Z.; Lomeda, J.; Tour, J. Soluble graphene through edge-selective functionalization. *Nano Res.* **2010**, *3*, 117–125.

37 Boukhvalov, D. W.; Katsnelson, M. I.; Lichtenstein, A. I. Hydrogen on graphene: Electronic structure, total energy, structural distortions and magnetism from first-principles calculations. *Phys. Rev. B* **2008**, *77*, 035427.

38 Gao, H.; Wang, L.; Zhao, J.; Ding, F.; Lu, J. Band Gap Tuning of Hydrogenated Graphene: H Coverage and Configuration Dependence. *J. Phys. Chem. C* **2011**, *115*, 3236–3242.

39 Lebegue, S.; Klintenberg, M.; Eriksson, O.; Katsnelson, M. I. Accurate electronic bandgap of pure and functionalized graphane from GW calculations. *Phys. Rev. B* **2009**, *79*, 245117.

40 Bloch, F. Zum elektrischen Widerstandsgesetz bei tiefen Temperaturen. *Z. Phys. A: Hadrons Nucl.* **1930**, *59*, 208–214.

41 Grüneisen, E. Die Abhängigkeit des elektrischen Widerstandes reiner Metalle von der Temperatur. *Ann. Phys.* **1933**, *408*, 530–540.

42 Cançado, L. G.; Takai, K.; Enoki, T.; Endo, M.; Kim, Y. A.; Mizusaki, H.; Jorio, A.; Coelho, L. N.; Magalhães-Paniago, R.; Pimenta, M. A. General equation for the determination of the crystallite size La of nanographite by Raman spectroscopy. *Appl. Phys. Lett.* **2006**, *88*, 163106.

43 McCann, E.; Kechedzhi, K.; Fal'ko, V. I.; Suzuura, H.; Ando, T.; Altshuler, B. L. Weak-Localization Magnetoresistance and Valley Symmetry in Graphene. *Phys. Rev. Lett.* **2006**, *97*, 146805.

44 Moser, J.; Tao, H.; Roche, S.; Alzina, F.; Sotomayor Torres, C. M.; Bachtold, A. Magnetotransport in disordered graphene exposed to ozone: From weak to strong localization. *Phys. Rev. B* **2010**, *81*, 205445.

45 Sun, Y. Y.; Kim, Y.-H.; Lee, K.; Zhang, S. B. Accurate and efficient calculation of van der Waals interactions within density functional theory by local atomic potential approach. *J. Chem. Phys.* **2008**, *129*, 154102.